Near-Term Effects of the Lower Atmosphere in Simulated Northwest Flow Snowfall Forced over the Southern Appalachians

DOUGLAS K. MILLER

Department of Atmospheric Sciences, University of North Carolina at Asheville, Asheville, North Carolina

(Manuscript received 15 September 2011, in final form 14 May 2012)

ABSTRACT

Northwest flow snowfall (NWFS) impacts the southern Appalachian Mountains after the upper-level trough has departed from the region, when moist northwesterly flow near the ground is lifted after encountering the mountains. Snowfall associated with these events is highly localized and challenging to predict as the clouds generating the accumulation are mesoscale in structure and depend on rapidly varying structures of moisture, instability, and wind in the planetary boundary layer (PBL) and on the relief of the local topography. The purpose of this study is to investigate the near-term impact of heat and moisture fluxes at the ground on the evolution of an NWFS event using several simulations of the Advanced Research core of the Weather Research and Forecasting mesoscale model. Model simulations indicate that convective banding is responsible for the snowfall accumulations in the southern Appalachians during the event and the structure of the banding is sensitive to the vertical positions of maximum wind shear and minimal stability within the PBL. Sensible heat fluxes at the ground upstream of the mountains in the daytime tend to deepen the PBL, reduce cloud water content, and reduce snowfall accumulations. At the same time, however, the daytime sensible heating also increases the overall vapor of the PBL through increased turbulent mixing and the transport of vapor made available to the atmosphere through upward latent heat fluxes at the ground. Latent heat fluxes at the ground upstream of the southern Appalachian Mountains provide a source of moisture that contributes a significant fraction of the overall simulated snowfall accumulations.

1. Introduction

The purpose of this study is to investigate the near-term impact of heat and moisture fluxes at the ground directly upstream of the southern region of the Appalachian Mountains (SAMs) on snowfall accumulation in the SAMs through experiments using the Advanced Research core of the Weather Research and Forecasting (ARW-WRF) mesoscale model. Specifically, this study seeks to investigate the potential impact of antecedent surface conditions upstream of the SAMs for a northwest flow snowfall (NWFS) event that occurred early in the 2010/11 cool season. The study is unique in that it focuses on the near-term (both in space and time) effects of surface sensible heat (SH) and latent heat (LH) fluxes on the simulated 24-h NWFS accumulation over the SAMs and narrows the focus to fluxes occurring over land.

Snowfall over the SAMs (thickened box in Fig. 1) sometimes occurs with northwest synoptic-scale flow (Perry and Konrad 2006). These NWFS events can account for 50% of the mean annual snowfall at high altitudes along the windward slopes of the southern Appalachians (Perry 2006; Perry et al. 2010). These events often occur after the passage of the upper-level trough, when quasigeostrophic forcings are generally unfavorable for precipitation generation. In these cases, mechanically forced lift along the mountain barrier is the precipitation generation mechanism. In some instances, buoyant convection can become dominant once parcels reach their level of free convection through terrain-induced lift. In addition, moist-layer temperatures during passage of the upper-level trough are typically quite cold in the moist layer, in the range −14° to −17°C, favorable for dendritic snow crystal growth (Ryan et al. 1976; Pruppacher and Klett 1997; Fukuta and Takahashi 1999). A unique collaboration has been

Corresponding author address: Dr. Douglas K. Miller, Dept. of Atmospheric Sciences, University of North Carolina at Asheville, CPO 2450, One University Heights, Asheville, NC 28804.
E-mail: dmiller@unca.edu

DOI: 10.1175/WAF-D-11-00103.1

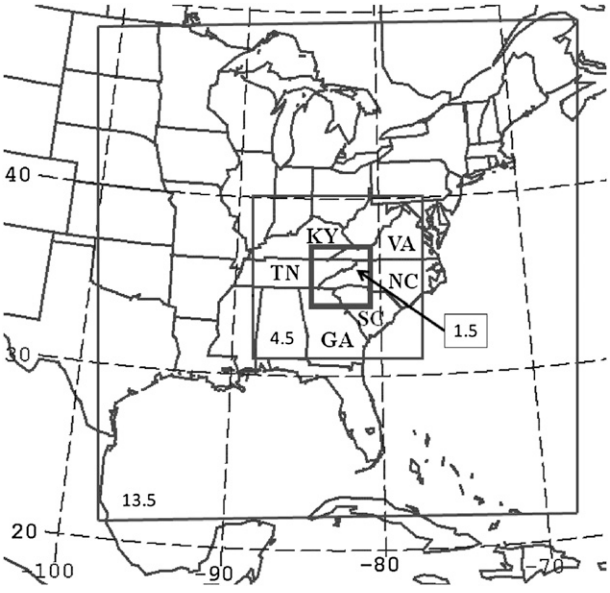

FIG. 1. Study region centered on the SAMs. Three nested model domain configurations highlighted by the boxes, with labels showing corresponding horizontal grid spacing (km) for each domain. The thickened box corresponds to the innermost model domain (horizontal grid spacing of 1.5 km) and is the primary focus of the model-simulated accumulated precipitation.

formed to better understand and predict NWFS events and is described in Keighton et al. (2009).

The challenge in predicting snow accumulation with NWFS is that it is highly localized due in part to the topographic relief variability of the mountains (Perry and Konrad 2006) and to the mesoscale variability of the low-level atmospheric moisture, temperature, and stratification (Perry and Konrad 2006; Holloway 2007; Keighton et al. 2009). Observations of clouds generating NWFS by a vertically pointing micro–rain radar (Yuter and Perry 2007; Keighton et al. 2009) indicate that they are extremely shallow, with tops rarely exceeding 2000 m above ground level. The mesoscale variability of the low-level atmosphere is due in part to the different synoptic conditions that generate NWFS events. Perry et al. (2010) list several synoptic condition categories favorable for producing NWFS.

Considerable variability in the low-level atmospheric structure occurs during a single NWFS event. Snow-to-liquid ratios (SLRs) can range from 10:1 just after passage of the surface cold front to over 40:1 a few hours (or days) later (Perry et al. 2008). Other factors impacting NWFS accumulations are transiting short waves through the upper-level trough, arrival of moisture packets (a discrete collection of saturated air parcels) at low levels, and an evolving planetary boundary layer (PBL) responding to the movement of short waves aloft (e.g., Lackmann 2001) and to the changing surface conditions typical of a diurnal cycle. An influence found to be important for snowfall accumulations near the Great Lakes (e.g., Sousounis 2001) that may also be relevant to NWFS events is the strength and height of the capping inversion.

The arrival of moisture packets at low levels in ''classical'' NWFS events is particularly noteworthy in cases whose upwind trajectories extend to the Appalachian Mountains southeastward from the Great Lakes (Schmidlin 1992; Sousounis and Fritsch 1994; Holloway 2007; Perry et al. 2007; Keighton et al. 2009). These moisture packets are distinct from upper-level moisture that might be wrapping around the synoptic-scale surface low pressure center usually located near the northeastern United States. The Great Lakes moistening influence as analyzed using the ARW-WRF mesoscale model simulations has shown significant variability between events (Holloway 2007). Some events showed lower sensitivity to moistening effects, but revealed that the lakes can also influence NWFS accumulations through heating of the PBL and the related destabilization of the lower troposphere. The warming of low-level air parcels by the lakes reduced atmospheric stratification and indirectly contributed to the ability of parcels within northwest flow to ascend the SAMs, enhancing orographic lift and increasing NWFS accumulation.

Hudgins (2008) and Keighton et al. (2009) noted the evolving NWFS cloud structures sometimes change from cellular types during daytime hours to banding during the nighttime hours. The bands can extend far downstream from the mountain ridgelines, resulting in higher snow accumulations on the leeward sides of mountains. The change in convective cloud types between bands and rolls can reflect the diurnal variations in the depth of the PBL (Weckwerth et al. 1999) with cells or unorganized cloud patterns becoming the dominant pattern during the daytime, coinciding with a deeper PBL. The banding often resembles cloud streets (a.k.a. horizontal convective rolls) that are indicative of strong vertical wind shear and moderate convective PBL instability (Stull 1988). The aspect ratio (horizontal to vertical) of cloud streets is determined primarily by the convective BL depth according to linear theory (Brown 1980), with larger aspect ratios occurring for larger convective BL depths (Young et al. 2002). Orographic precipitation banding has been attributed to fluid instabilities beyond that responsible for cloud streets, related to the upstream flow properties of low-level vertical wind shear and stability (Kirshbaum and Durran 2005; Kirshbaum et al. 2007a,b).

Given that NWFS cloud structures are sensitive to the low-level stratification and moisture of the upstream environment, a hypothesis being explored in this study is

that soil moisture conditions upstream of the mountains can contribute to a higher NWFS snowfall accumulation event if the soil contains elevated amounts of groundwater from recent rainfall or snowmelt and no snow covers the ground. A second hypothesis being examined is that the intensity of cloud and precipitation formation during NWFS events can be significantly influenced by diurnal effects in the PBL. The remainder of this manuscript is organized as follows. A description of the study methodology is provided in section 2, a brief summary of the synoptic-scale conditions of the 6/7 December 2010 NWFS event is described in section 3, an analysis of the ARW-WRF model simulation results for the case study is given in section 4, and a summary of the findings and their implication for making improved near-term NWFS accumulation forecasts is described in section 5.

2. Methodology

A series of numerical experiments was conducted on the 5–8 December 2010 NWFS event using version 3.1.1 of the ARW-WRF mesoscale model (Skamarock et al. 2008). The simulations consisted of three one-way nested model domains centered on a point in the SAMs (Fig. 1), whose horizontal grid spacings were defined to be 13.5, 4.5, and 1.5 km for the outer, middle, and innermost nests, respectively. The 45 model vertical levels of the three domains extended from the ground to the model top at the 100-hPa level. The specified model physics used were the WRF single-moment five-class microphysics (WSM5) explicit moisture scheme (Hong et al. 2004; Hong and Lim 2006), the Monin–Obukhov similarity theory–based surface-layer scheme linked with the Yonsei University PBL scheme (Hong et al. 2006), the unified Noah land surface model with four soil layers, the Betts–Miller–Janjić convective parameterization scheme (Janjić 1994, 2000) switched ''on'' for only the two outer domains (13.5 and 4.5 km), and the Rapid Radiative Transfer Model (RRTM) longwave (Mlawer et al. 1997) and Eta Geophysical Fluid Dynamics Laboratory shortwave radiation schemes.

The ARW-WRF simulations were integrated for 48 h using initial conditions and lateral boundary conditions (6-h updates) from the National Centers for Environmental Prediction's (NCEP) North American Regional Reanalysis (NARR; Mesinger et al. 2006) project obtained online (http://nomads.ncdc.noaa.gov/data.php). The initial conditions were generated using the WRF Environmental Modeling System (EMS; Rozumalski 2007) version 3.1 software for the model start time at 0000 UTC 6 December 2010.

The ARW-WRF experiments in this study involved running ''SH off'' or ''LH off'' during the first 12-h period of the model simulation (P1), during the middle 12-h period of the model simulation (P2), or during the final 24-h period of the model simulation (P34). The remainder of the model time integration consisted of using either the ''default,'' ''50% SH enhancement,'' or ''50% LH enhancement'' unified Noah land surface model. The surface sensible and latent experiment simulations were run separately so that the impacts of surface warming and surface moistening could be assessed in a more straightforward manner. The enhanced experiments involved multiplying the default estimate by 1.5, changing the magnitude of the surface moisture or heat fluxes without modifying their direction. The enhanced experiments were included to investigate the impacts on NWFS accumulation predictions in the event that the default land surface model had a low flux magnitude (damped) bias either due to imperfect model physics (e.g., transfer coefficient underestimate) or to a poor surface moisture or temperature initialization. Errors in observations of surface moisture or heat fluxes of 50% are not unusual (e.g., Stearns and Weidner 1993).

The majority of the model simulation analysis utilizes forecast fields from the 4.5- and 1.5-km (thickened box in Fig. 1) domains, whose terrain depictions by the ARW-WRF are shown in Figs. 2a and 2b, respectively. Locations of the Cumberland Plateau and Great Smoky Mountains in the SAMs are noted in Fig. 2a as are the locations of Knoxville, Tennessee; Asheville, North Carolina; and the nearby Automated Surface Observing System (ASOS) station at the Asheville Regional Airport (KAVL) relative to the SAMs in Fig. 2b. Also highlighted in Fig. 2b is Max Patch, situated between Knoxville and Asheville, the location receiving the greatest simulated 24-h accumulation during the final 24-h period (P34) of the default ARW-WRF 48-h model run ending at 0000 UTC 8 December 2010.

3. Synoptic conditions

The 5–8 December 2010 NWFS event was chosen to study for two reasons. It was potentially driven, in part, by surface conditions in which the land surface over the central and eastern United States had not yet become frozen and covered with snow. A significant synoptic-scale rain event impacted the central and eastern United States on 29–30 November 2010, resulting in nearly saturated soil conditions and many isolated incidents of flooding and flash flooding (NCDC 2010a). The region immediately upstream of the SAMs in Kentucky and Tennessee received over 1.5 in. of rainfall from 1200 UTC 30 November to 1200 UTC 1 December 2010. The NWFS event of this study occurred less than 1 week later, so the soil conditions upstream of the SAMs still

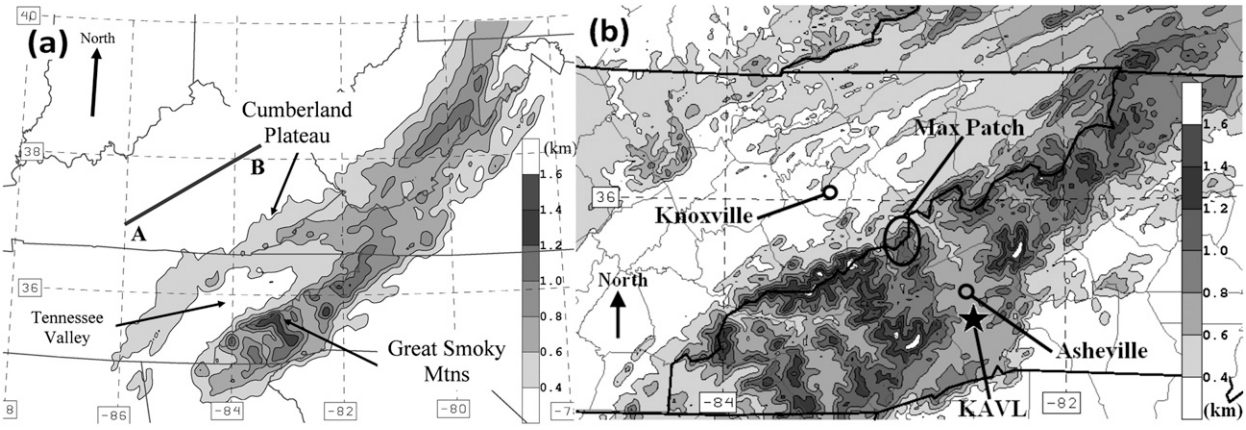

FIG. 2. Nested (a) 4.5- and (b) 1.5-km domain terrain elevations (km) exceeding 0.4 km above sea level. Line marked A–B in (a) is the orientation of the vertical cross section shown in Fig. 16 located upwind of the SAMs. Locations of the Cumberland Plateau and Great Smoky Mountains of the SAMs are noted in (a), as are the locations of Knoxville (circle), Asheville (circle), and the nearby KAVL ASOS station (star) relative to the SAMs in (b). Also highlighted in (b) is Max Patch (oval), situated between Knoxville and Asheville, the location receiving the greatest simulated 24-h accumulation during the final 24-h period (P34) of the ARW-WRF 48-h model run ending at 0000 UTC 8 Dec 2010.

had significant moisture content at the time of its onset, as confirmed from soil moisture observations at two Natural Resources Conservation Services stations in western and central Kentucky, which indicated elevated amounts compared to their pre–30 November 2010 levels.

A second reason that the 5–8 December 2010 NWFS event was chosen for study was due to its relatively significant impact on the residents of western North Carolina. Most of the school districts in the region, including the county district serving the suburbs of Asheville (Buncombe County School District), were forced to close on 7 December due to bitterly cold weather and poor road conditions arising from the snowfall accumulation that occurred overnight on 6/7 December (*Asheville Citizen-Times,* 8 December 2010). Amounts ranged from about 2 to 6 in. of snow in the valleys of the Tennessee border counties, to 10 in. at the high elevations of the Smoky Mountains, to almost 18 in. in the mountains farther to the north of the Smoky Mountains in North Carolina (NCDC 2010b).

At 1800 UTC 4 December 2010 [1300 eastern standard time (EST) 4 December 2010] light rain was observed at the KAVL ASOS station (position indicated by the star in Fig. 2b). KAVL is located in a river valley in southern Buncombe County that typically experiences minimal NWFS effects. The cold front passed Asheville at 0000 UTC 5 December and light snow was reported at KAVL starting at 1400 UTC 5 December, by which time the NWFS event can be defined to have started at Asheville. Snowfall associated with the NWFS portion of the event was over by 0000 UTC 8 December.

The 5–8 December 2010 NWFS event falls within the SE category of synoptic conditions bringing snowfall to the Great Smoky Mountains, as described by Perry et al. (2010), in which a southeastward-tracking short wave, marked by a vorticity maximum at the 500-hPa level (Fig. 3), brings snow to the region via upslope or northwest flow near the surface (Fig. 4). The 500-hPa-level thermal and geopotential wave at 1200 UTC 7 December shows the SAMs region to be covered by arctic air, with the primary upper-level trough having already propagated well to the east. The short wave embedded in the large-scale trough may have enhanced the synoptic-scale lift overnight on 6/7 December and contributed to significant snowfall accumulations observed for the SAMs.

An area of pronounced cloud coverage marks the advance of the embedded short wave in the upper-level trough in *GOES-13* visible satellite (Fig. 5) and Next Generation Weather Radar (NEXRAD; Fig. 6) imagery. The sky is relatively clear in the early daylight hours (1602 UTC, Fig. 5a), with transverse-oriented cloud banding (parallel to the ridgelines), suggestive of trapped or resonant lee waves (Durran 1986). Later during the daylight hours (1902 UTC, Fig. 5b) the region in eastern Kentucky and Tennessee has become increasingly overcast with longitudinally oriented cloud bands having formed, oriented along the northwesterly flow direction, in addition to the transverse bands. After sunset (0206 UTC, Fig. 6), the longitudinal banding becomes more isolated with the largest bands confined to the North Carolina–Tennessee border forced primarily by upslope flow at the SAMs, after the embedded short wave has moved downstream of the study region.

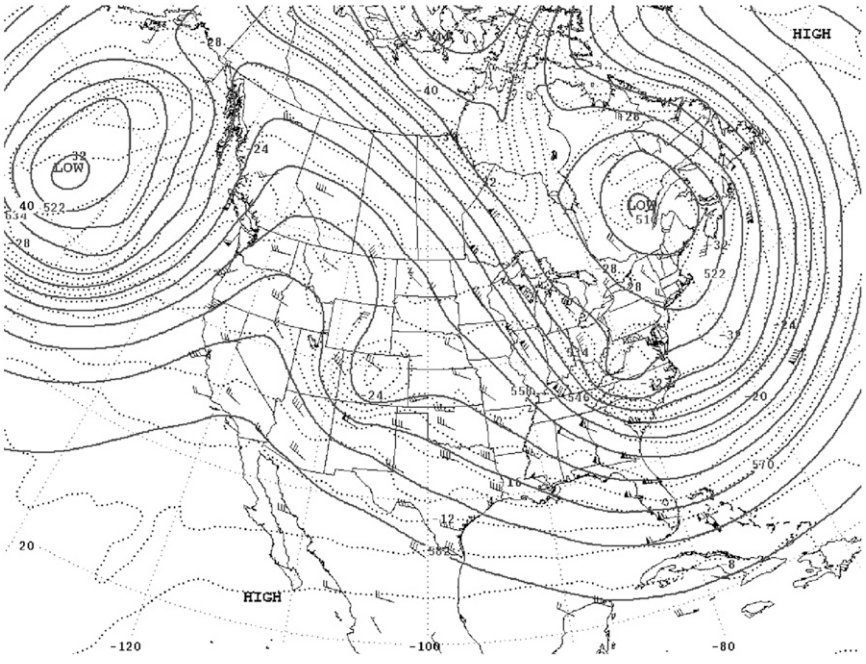

FIG. 3. Daily weather map of geopotential height (solid contours, interval = 60 m) and temperature (dashed contours, interval = 2°C) at the 500-hPa level available from the Hydrometeorological Prediction Center (HPC) valid 1200 UTC 7 Dec 2010. (Courtesy of the HPC.)

4. Results

Model-simulated 3-h liquid equivalent accumulated precipitation (cm) with the default unified Noah land surface model for a location near Max Patch (35.79°N, 82.97°W, elevation ~1200 m) starting at 0000 UTC 6 December 2010 is depicted in Fig. 7. This location corresponded to the grid point having the highest 24-h accumulation in the 1.5-km domain for the 0000 UTC 7 December –0000 UTC 8 December period (P34): 1.64-cm

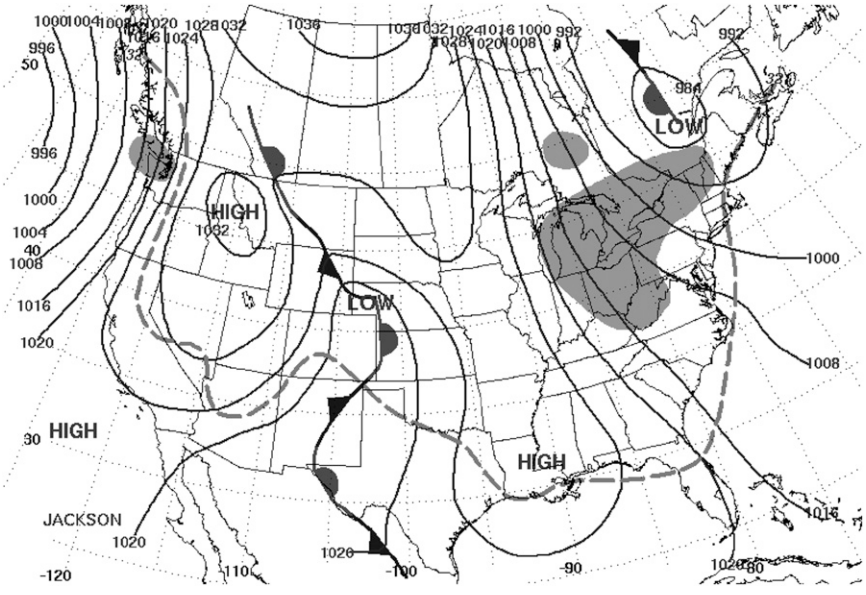

FIG. 4. Daily weather map of mean sea level pressure (solid contours, interval = 4 hPa), 0°C isotherm (dashed), locations of overcast skies (shading), and surface fronts available from the HPC valid 1200 UTC 7 Dec 2010. (Courtesy of the HPC.)

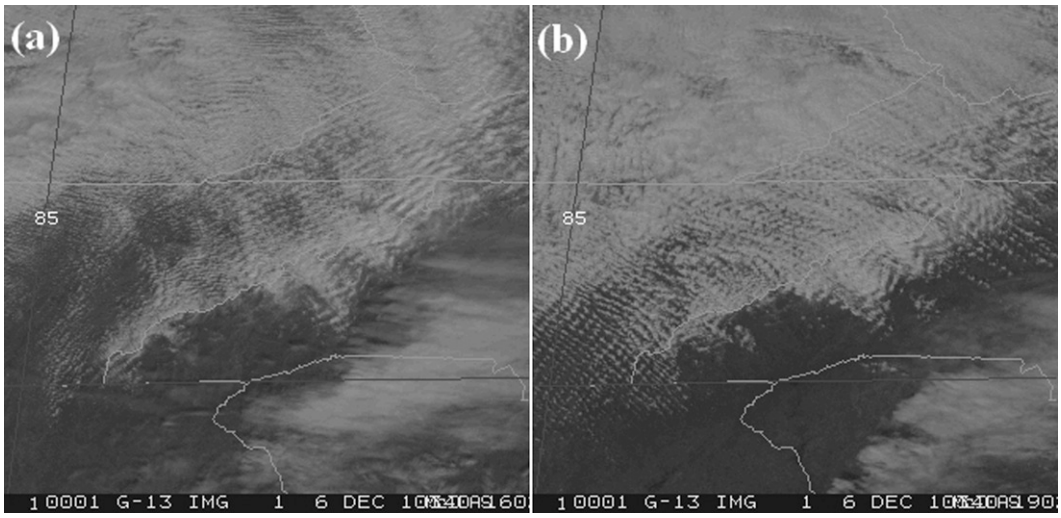

FIG. 5. *GOES-13* visible imagery valid (a) 1602 and (b) 1902 UTC 6 Dec 2010. [Courtesy of the National Climatic Data Center (NCDC).]

(0.6 in.) liquid equivalent. Observations during this period indicated a SLR of approximately at most 40:1 (L. B. Perry 2011, personal communication) so that the simulated liquid equivalent precipitation translates to an upper-limit 24-h snowfall accumulation of 65.6 cm (24 in.) near Max Patch. Investigation of simulated and observed liquid water equivalents at several locations in eastern Tennessee and western North Carolina indicates that the WRF default simulation is providing a realistic range of values. It is possible that the simulated accumulation near Max Patch is an overestimate compared to any location within the SAMs; however, this cannot

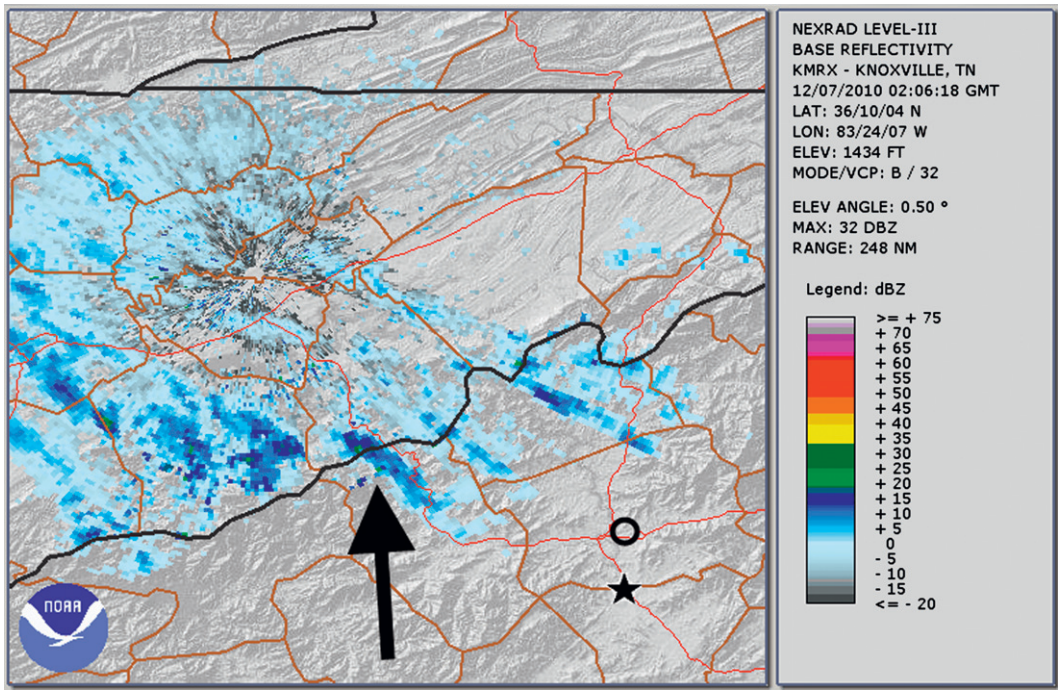

FIG. 6. Reflectivity at the lowest elevation scan (0.50°) of the KMRX NEXRAD observations valid 0206 UTC 7 Dec 2010, clear-air mode. The circle symbol highlights the location of Asheville, the star symbol is the location of KAVL, and the arrow notes the position of a dominant snowband at the time of the NEXRAD scan. (Courtesy of the NCDC.)

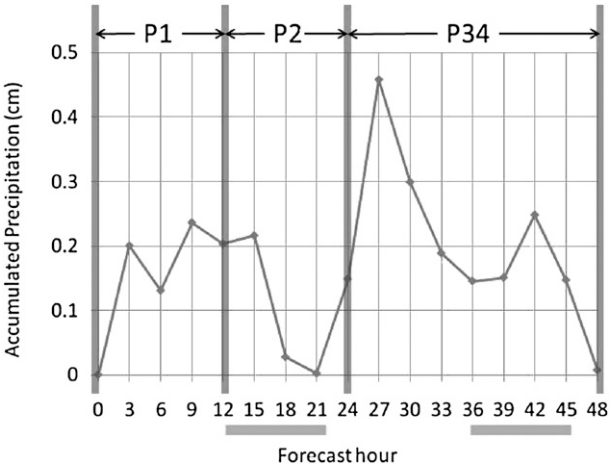

FIG. 7. Innermost (1.5 km) domain model simulated 3-h accumulated precipitation (cm) for a location near Max Patch (35.79°N, 82.97°W; see Fig. 2b for location) starting at 0000 UTC 6 Dec 2010. Designators P1, P2, and P34 of 12-h study periods are also indicated. Horizontal thick lines indicate the period associated with daylight hours (sunrise, 0725 EST; sunset, 1717 EST).

be known with a high degree of confidence due to the spatial gaps in high quality accumulation observations. The validity of the WRF default simulation for the December 2010 case study is primarily confirmed by the accurate handling of the macroscopic cloud properties of the event described at the end of section 3.

Daytime hours for the SAMs during the December 2010 event are indicated by the thick horizontal lines near the bottom of the plot in Fig. 7. The model simulation indicates a significant dropoff in snowfall accumulation at Max Patch during the daytime hours on 6 December and a rather dramatic increase in accumulation corresponding to the nighttime hours overnight on 6/7 December. Snowfall then gradually diminishes, with the exception of the 42-h forecast (1800 UTC 7 December 2010), as the favorable low-level moisture and temperature conditions exit the area. Of interest will be an examination of the role of surface warming or cooling in the simulated daytime–nighttime accumulation differences between the daytime hours on 6 December and the overnight hours that followed, potentially adding insight to observations of diurnal differences in cloud evolution noted by Hudgins (2008) and Keighton et al. (2009).

The study region during the period leading up to the 24-h period of interest (P34) is characterized synoptically by large-scale subsidence in the wake of the 500-hPa trough passage (Fig. 8). However, a short wave is evident over Wisconsin at 1200 UTC 6 December [Fig. 8a, corresponding to the 12-h forecast (F12)] that propagates through the 500-hPa wave so that it is over the study region 12 h later [Fig. 8b, corresponding to the 24-h forecast (F24)] and contributes to localized ascent due to vertical differential cyclonic vorticity advection.

A model sounding located at the center of line A–B (noted in Fig. 2a) upstream of the Cumberland Plateau (Fig. 9) valid at 2000 UTC 6 December 2010 indicates a well-mixed PBL from the surface to the 850-hPa level. Vapor mixing ratios exceeding 1.4 g kg^{-1} are confined to a shallow layer below the 850-hPa level, typical of NWFS events (Keighton et al. 2009), and the moist layer is capped by a stable layer associated with large-scale subsidence. Nearly unidirectional northwesterly flow is evident from near the ground through the 100-hPa level.

The model-simulated cloud and hydrometeor (liquid + ice) mixing ratio at the 850-hPa level is used in Fig. 10 to depict the horizontal evolution of precipitation-generating clouds over the study region every 3 h from

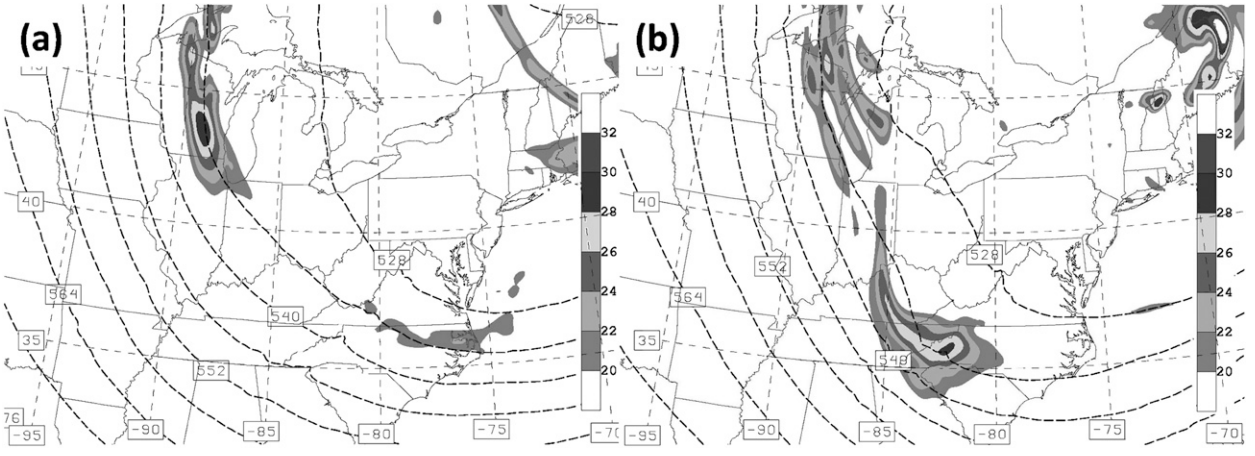

FIG. 8. Outermost (13.5 km) domain model simulated 500-hPa level geopotential height (contoured in dashed lines every 6 dm) and absolute vorticity (shading, $\times 10^{-5}$ s^{-1}) valid at (a) 1200 UTC 6 Dec (F12) and (b) 0000 UTC 7 Dec 2010 [F24].

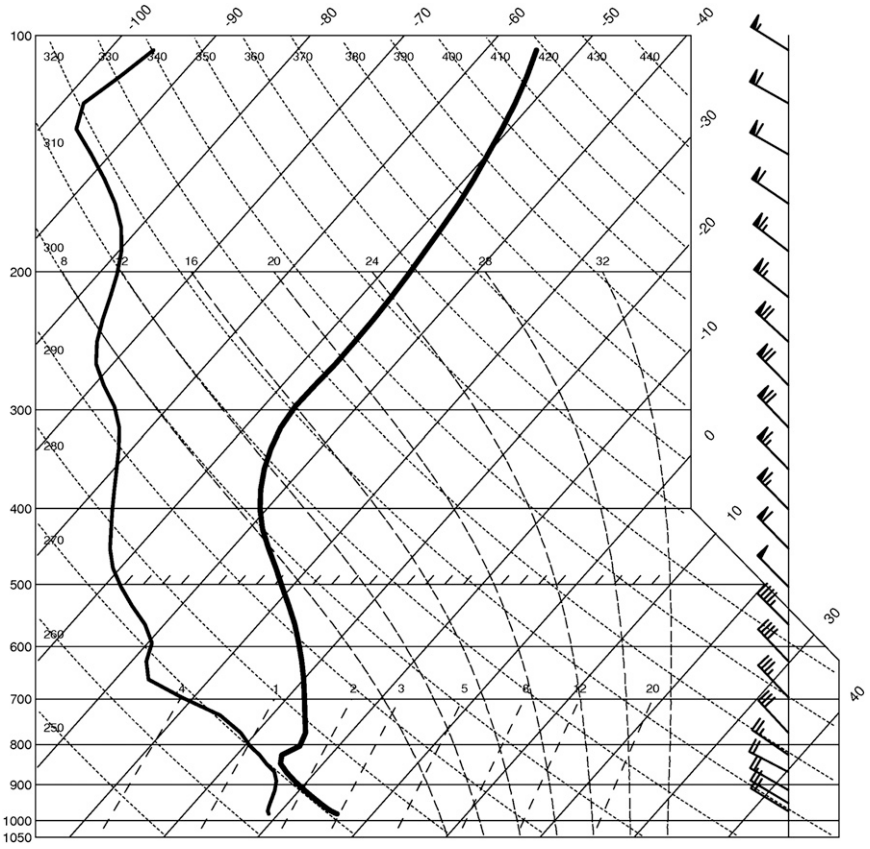

FIG. 9. Middle (4.5 km) domain model simulated skew *T*–log*p* diagram valid at 2000 UTC 6 Dec 2010 (F20) at the middle point of the upstream section location labeled A–B in Fig. 2a.

1800 UTC 6 December through 0300 UTC 7 December, the period up to and including the heaviest simulated precipitation at the Max Patch location (Fig. 7). The precipitating clouds have reached the extreme northwest corner of the study region, over the Cumberland Plateau, and are organized in bands oriented parallel both to the mean wind and shear vector directions at 1800 UTC 6 December (Fig. 10a).

Three hours later (Fig. 10b), both transverse and longitudinally oriented cloud features are evident and cover about half the study domain, a pattern similar to what was noted in the *Geostationary Operational Environmental Satellite-13* (*GOES-13*) image valid at 1902 UTC 6 December (Fig. 5b). By 0000 UTC 7 December (Fig. 10c), the banding has shifted primarily to the ridgelines associated with the Great Smoky Mountains and the mountains near Max Patch, and a large band has evolved overhead of the latter location, stretching downwind over central Buncombe County. At 0300 UTC 7 December (Fig. 10d), the cloud structure is similar to what was simulated 3 h earlier, but the cloud banding is more localized in nature, as can also be seen in the Knoxville (KMRX) NEXRAD imagery valid 0206 UTC 7 December (Fig. 6). In contrast, the primary cloud band evident in the NEXRAD image (highlighted by the arrow) is located almost 15 km to the southwest of Max Patch along the North Carolina–Tennessee border.

From 1800 UTC 6 December through 0000 UTC 7 December, the dominant cloud structures follow the cyclonic vorticity advection downstream of the 500-hPa absolute vorticity maximum evident in Fig. 8. Once the banding shifts to the higher ridgelines associated with the Great Smoky Mountains and near Max Patch at 0000 UTC 7 December, more localized effects appear to maintain the bands and their associated precipitation. Also of note is the increase in horizontal spacing between the cloud bands from 2100 UTC 6 December to 0000 UTC 7 December, two periods representing daylight and nighttime hours, respectively. The cooling PBL after sunset at 2217 UTC 6 December (1717 EST) happens to be coincident with the changing organization of the cloud bands, in addition to the influence of the 500-hPa cyclonic vorticity maximum moving out of the domain by 0000 UTC 7 December.

Twenty-four-hour trajectories from the Hybrid Single-Particle Lagrangian Integrated Trajectory (HYSPLIT;

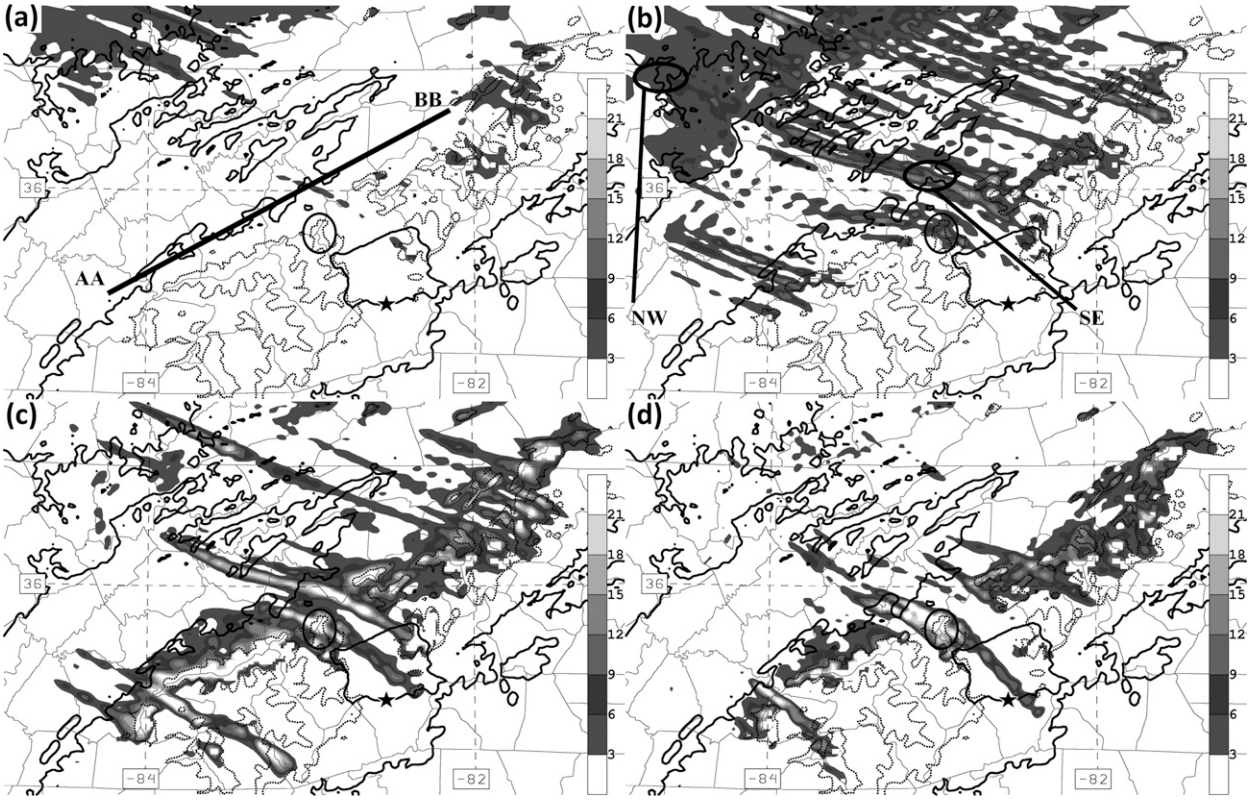

FIG. 10. Innermost (1.5 km) domain model simulated 850-hPa-level liquid and ice mixing ratio (shading, $\times 10^{-2}$ g kg^{-1}) and terrain elevation exceeding 0.4 (thick solid contours) and 1.0 km (dotted) valid at (a) 1800 UTC 6 Dec (F18), (b) 2100 UTC 6 Dec (F21), (c) 0000 UTC 7 Dec (F24), and (d) 0300 UTC 7 Dec 2010 (F27). Line AA–BB in (a) represents the ending locations of the trajectories displayed in Fig. 11. A band whose endpoints are labeled NW–SE in (b) shows the orientation of the vertical cross section displayed in Figs. 12 and 14. The borders of Buncombe County are thickened and the star symbol highlights the location of KAVL at the southern boundary of the county. The location of Max Patch is indicated by an oval to the northwest of Buncombe County.

Draxler and Hess 1998, 1997) model based on the 13.5-km-domain wind forecasts for the three air parcels ending at the far left (AA), middle point, and far right (BB) locations at the midcloud (850 hPa) level are traced in Fig. 11. Close inspection of the horizontal trajectories (Fig. 11, top) makes clear that the 5–8 December 2010 NWFS event does not tap directly into the moisture or destabilizing effects of the Great Lakes. Each of the parcels ending up in the orographically enhanced cloud at 0000 UTC 7 December had their origins over Illinois or Iowa and were located in the PBL during their entire journey to the SAMs region.

A vertical cross section oriented along the longitudinal band labeled NW–SE in Fig. 10b shows periodic vertical motion downstream of the Cumberland Plateau in Fig. 12 associated with the transverse waves apparent in the enhanced cloud moisture shaded in Fig. 10b. The upright nature of the vertical motion maxima and minima is suggestive of trapped or resonant lee waves (Durran 1986) and occurs only when the Scorer parameter (Scorer 1949) decreases with height. Calculation of the Scorer parameter for the sounding at the upstream location depicted in Fig. 9 above the cloud layer indeed satisfies Scorer's resonance condition, indicative of an environment favorable for trapped lee waves. The cloud top shown in the vertical section corresponds to the bottom of the inversion layer and so the cloud is entirely contained in the conditionally unstable PBL, below about the 800-hPa level.

a. Surface sensible heat flux experiments

The purpose of the surface sensible heat flux experiments is to identify potential impacts on NWFS events due to diurnal heating and cooling impacts at the surface. For each of the experiments applied to the December 2010 case study, the direction of the sensible heat fluxes (not shown) is almost continually such that heat is being lost by the ground to the colder atmosphere in the daylight hours when the land surface model is ''on.'' Therefore, the enhanced sensible heat flux experiments generally increase the instability of the PBL in the daylight hours compared to the default simulations.

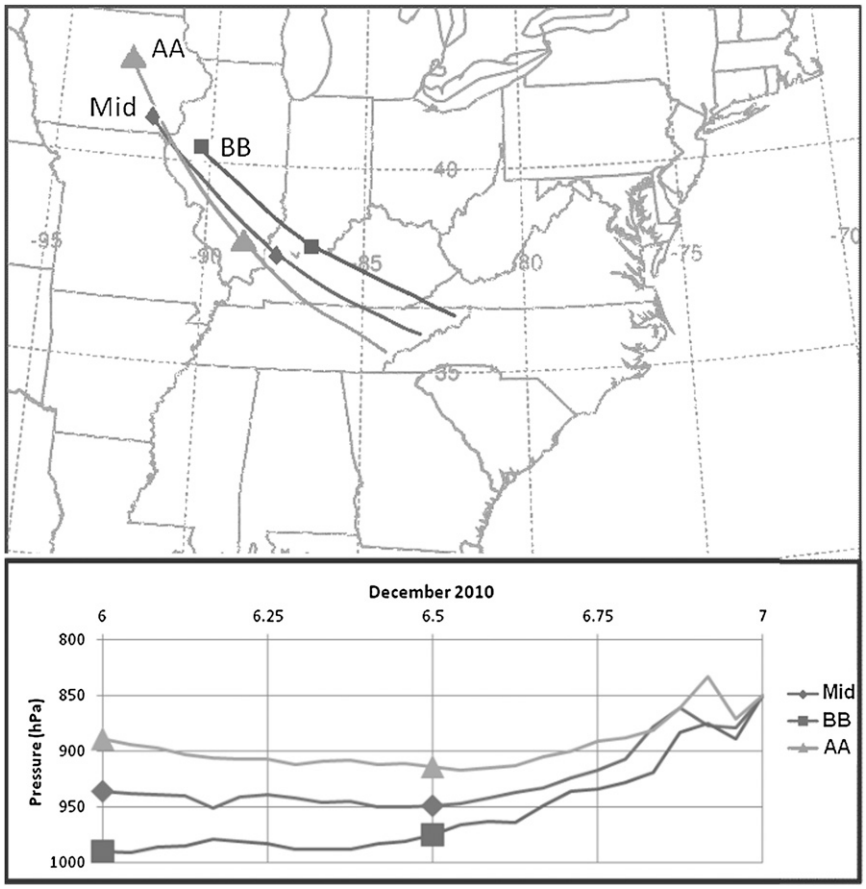

FIG. 11. Outermost (13.5 km) domain model simulated 24-h trajectories (0000 UTC 6/7 Dec 2010) analyzed by HYSPLIT for air parcels ending at the endpoints [AA, filled triangles (▲); BB, filled squares (■)] and the middle point [Mid, filled diamonds (◆)] of the section location shown in Fig. 10a at the 850-hPa level (middle of the cloud layer).

Model-simulated 24-h liquid equivalent accumulated precipitation for the period ending 0000 UTC 8 December 2010 (P34) is shown for four surface SH flux experiments in Fig. 13. The simulations show the most significant accumulations, exceeding 0.50 cm of liquid equivalent, occurring near the crest of the Great Smoky Mountains and the mountains near Max Patch. The elongated areas of accumulation oriented normal to the crest of these mountains are consistent with the banding nature of the clouds producing the precipitation. An accumulation exceeding 0.05 cm is found near KAVL and in southeastern Buncombe County, at least 43 km downwind of the primary mountain crest. In precipitation over mountainous regions, banding allows precipitation to extend much farther downstream of the mountain crest than if pure upslope was the dominant mode (Yoshizaki et al. 2000).

A statistical comparison of the final 24-h-period (P34) precipitation accumulation in the 1.5-km domain for the surface SH flux experiments is provided in Table 1 for grid points having accumulation amounts of at least 0.025 cm (1.0-cm snowfall accumulation for a 40:1 SLR). Table 1 shows the statistical comparisons corresponding to the model simulations shown in Fig. 13. The no surface SH flux simulation (off for *all* hours, Fig. 13d) has an overall greater accumulation over the study domain as reflected by a greater mean (0.163 cm), a comparable accumulation standard deviation (0.181 cm), and a systematically higher predicted accumulation amount (positive bias) compared with the default surface SH flux simulation (+0.035 cm). In contrast, the enhanced surface SH flux on for the entire simulation (Fig. 13b) has the lowest overall accumulation in the entire study domain with a small mean (0.145 cm) and a large negative bias (−0.042 cm).

Another region of significant accumulation occurs over the Cumberland Plateau in the northwest corner of the 1.5-km domain. Those experiments having surface

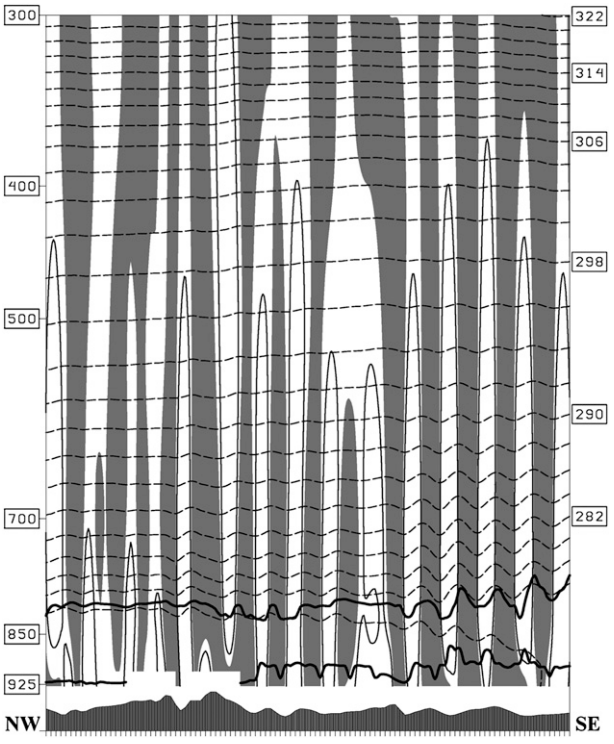

FIG. 12. Innermost (1.5 km) domain model simulated vertical motion (sinking motion shaded, rising motion exceeding 1.0 hPa s^{-1} contoured), cloud mixing ratio (thick solid contour, 1×10^{-2} g kg^{-1}), and potential temperature (contoured in dashed lines every 2 K) valid at 2100 UTC 6 Dec 2010 (F21) in a vertical cross section oriented along the cloud band labeled NW–SE in Fig. 10b. The horizontal distance between vertical motion crests is approximately 10 km.

SH fluxes shut off during the daytime hours (Figs. 13c and 13d) distribute greater amounts of snowfall over the Cumberland Plateau than do the experiments having surface SH fluxes on during daytime hours (Figs. 13a and 13b). This observation is supported by the statistics presented in Table 1 for the rows labeled relevant to the Cumberland Plateau (CP) region of the 1.5-km domain. The mean accumulation of the simulations having SH fluxes shut off during the daytime hours exceed the default simulation and show a systematically higher predicted accumulation amount (biases of +0.012 and +0.040 cm) for the CP region.

A comparison of the band-parallel vertical cross-section model simulations valid at 2100 UTC 6 December 2010 is provided in Fig. 14. The cloud band for the enhanced surface SH flux simulation (Fig. 14a) shows a uniformly higher PBL and cloud base and top compared to the default simulation (Fig. 12). The simulation having surface SH fluxes shut off throughout the simulation (Fig. 14b) reveals the opposite extreme of the default simulation with a uniformly shallower PBL and lower cloud base and top. In addition to having a deeper PBL, the enhanced surface SH flux simulation has a warmer (potential temperatures between 276 and 274 K) and slightly less stable PBL than either the default PBL (potential temperatures between 274 and 272 K) or the PBL of the simulation having surface SH fluxes shut off (potential temperatures between 272 and 268 K).

Close examination of the evolution of the clouds in the enhanced and zero-surface SH flux simulations reveals that their development in the former simulation is delayed such that almost no cloud covers the study domain at 1800 UTC 6 December (not shown). This delay is consistent with a warmer and deeper PBL noted in the analysis of the band-parallel sections (Fig. 14) compared with the other simulations, thereby requiring a greater amount of time to effectively mix the moisture throughout the PBL from the surface. The delay is part of the reason for smaller snowfall accumulations over the Cumberland Plateau depicted in Fig. 13b.

These results suggest that the *suppression* of surface sensible heat fluxes, particularly during the daylight hours, generally *increases* the simulated snowfall accumulation amounts. The simulation period designated ''P2'' corresponds to the daylight hours, when the PBL experiences its weakest stability, buoyancy-generated vertical mixing is maximized, and the unidirectional vertical wind shear, or shear-generated vertical mixing, in the lower PBL is minimized. The daytime sensible heat fluxes contribute to increasing the depth of the PBL, which effectively increases the volume of air that must become saturated before clouds can form at the top of the PBL, just beneath the bottom of the subsidence inversion. Hence, the daytime surface sensible heat fluxes partly oppose cloud development through the resultant heating and thickening of the PBL. However, the enhanced daytime mixing in the PBL also acts to efficiently transport moisture away from the ground, contributing to the moistening of air parcels in the PBL and working in concert with cloud development at the top of the PBL. It should be noted that the unidirectional vertical wind shear experienced during this event provides a nearly constant source of shear-driven mixing that helps to redistribute moisture through the PBL, independent of the time of day. The WRF model experiment in which surface sensible heat fluxes were shut off during the entire 48-h simulation (Fig. 13d) indicates that the shear-driven mixing is sufficient to moisten the air parcels in the PBL to supersaturation so that a significant amount of snowfall accumulation in western North Carolina is realized.

By 2100 UTC 6 December (Fig. 15), the cloud fields have evolved with significant differences compared to the default surface SH flux simulation (Fig. 10b). The

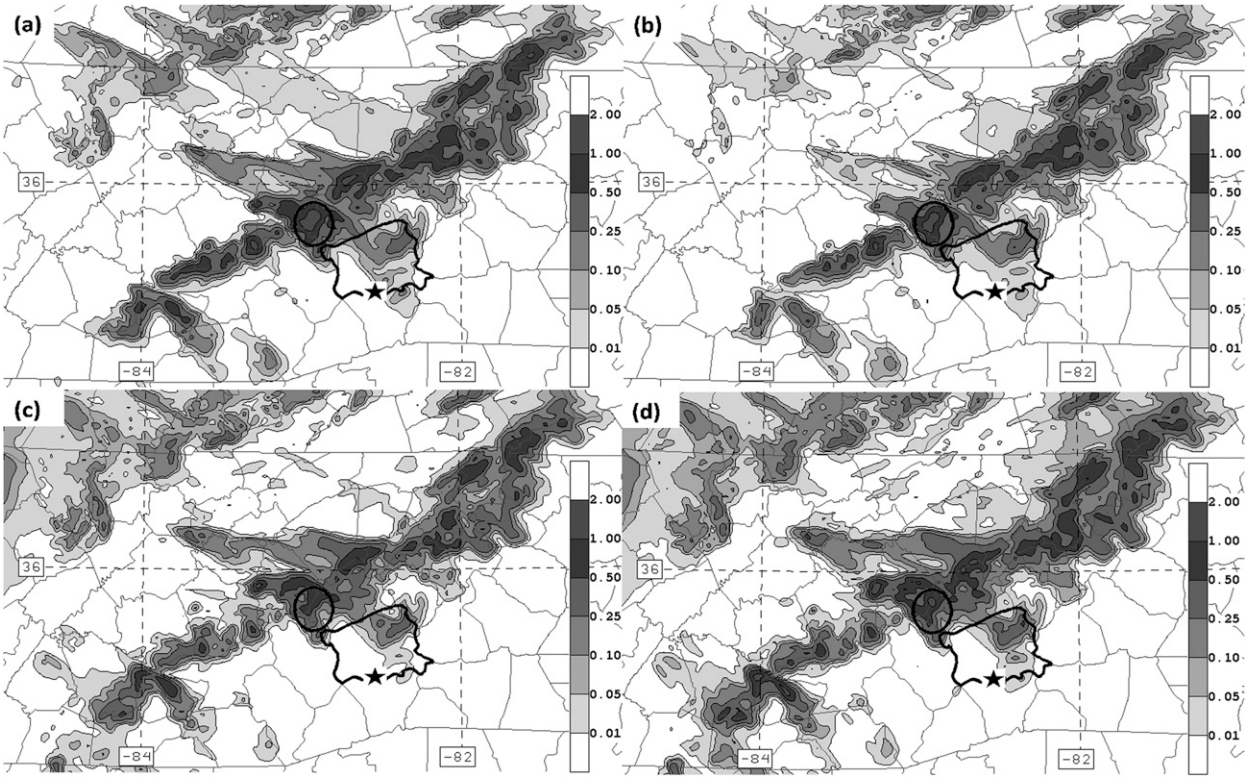

FIG. 13. Innermost (1.5 km) domain model simulated 24-h liquid equivalent accumulated precipitation (cm) for the period ending 0000 UTC 8 Dec 2010 (period designated P34) for the surface SH flux parameterization experiments having the (a) default SH flux parameterization scheme on during the entire model simulation, (b) enhanced SH flux parameterization scheme on during the entire model simulation, (c) default SH flux parameterization scheme off during P2, and (d) SH fluxes shut off during the entire model simulation. The borders of Buncombe County are thickened and the star symbol highlights the location of KAVL at the southern boundary of the county. The location of Max Patch is indicated by an oval to the northwest of Buncombe County.

enhanced and zero-surface SH flux experiments show differences in horizontal cloud spacing and cloud-mixing ratios in the middle of the simulated clouds (825-hPa level in Fig. 15a and 900-hPa level in Fig. 15b) over the northeastern Tennessee Valley. The zero-surface SH flux simulation has a wider spacing between bands, higher cloud mixing ratios within the bands, and wider cloud bands than the enhanced surface SH flux simulation. The lack of regular spacing between bands and the wide band spacing for a shallow convective PBL makes it doubtful that organizing processes typical of horizontal convective rolls are responsible for the simulated banding. The banding is also organized by mechanisms different from those explored in the idealized simulations of Kirshbaum et al. (2007b) in which the preferred band spacing decreases as the cloud base is lowered closer to the model orography.

A vertical cross section located upstream of the Cumberland Plateau in the 4.5-km domain (location shown in Fig. 2a) displaying atmospheric parameters that commonly determine the organization of orographic-driven convective banding (Kirshbaum and Durran 2005) is presented in Fig. 16 valid at 1800 UTC 6 December 2010. The conditionally unstable layer for the enhanced surface SH flux experiment having a lapse rate exceeding 9°C km^{-1} (shading in Fig. 16a) extends from the surface to above the 900-hPa level. This represents a deep well-mixed layer in the upstream environment as it approaches the plateau. The layer of strongest unidirectional vertical wind shear (represented by the 8 and 12×10^{-3} s^{-1} dashed contours) in the enhanced surface SH flux experiment is well elevated above the orography (at about the 825-hPa level) and coincides with the inversion capping the PBL. The conditionally unstable layer for the zero-surface SH flux experiment having a lapse rate exceeding 9°C km^{-1} (shading in Fig. 16b) extends from the surface to almost the 925-hPa level. The atmospheric flow upstream of the plateau for the zero-surface SH flux experiment is characterized by a highly stratified PBL, with the layer of strongest unidirectional vertical wind shear collocated with the most unstable PBL layer next to the ground. This near-surface

TABLE 1. Surface heat flux experiment statistics of the model-simulated 24-h liquid equivalent accumulated precipitation (cm) for the period ending 0000 UTC 8 Dec 2010. Only default and experiment grid points having at least one simulation whose 24-h liquid equivalent accumulated precipitation amount exceeding 0.025 cm are included in the statistics. The ''domain'' column defines the region within the 1.5-km domain for which the corresponding statistics are valid and abbreviation CP stands for Cumberland Plateau. The sixth column is the calculated standard deviation (cm), the seventh column is the root-mean-square difference (cm), the eighth column is the bias (cm, defined as the experiment minus the default simulation), and the final column is the total number of grid points in the calculations (out of 544 66 total grid points in the entire 1.5-km domain). Default model simulation results are highlighted in boldface and italicized font.

Figure	Surface SH flux parameter	SH scheme ''off''	Domain	Mean (cm)	σ (cm)	RMSD (cm)	Bias (cm)	N
13a	Default	Never	Entire	***0.187***	***0.204***	0.079	−0.042	10637
13b	50% enhancement	Never	Entire	0.145	0.185			
13a	Default	Never	Entire	***0.147***	***0.195***	0.113	−0.013	13635
13c	Default	P2	Entire	0.134	0.156			
13a	Default	Never	Entire	***0.128***	***0.187***	0.122	+0.035	15767
13d	Off	Always	Entire	0.163	0.181			
13a	Default	Never	CP	***0.095***	***0.073***	0.056	−0.041	2863
13b	50% enhancement	Never	CP	0.053	0.067			
13a	Default	Never	CP	***0.064***	***0.072***	0.053	+0.012	4441
13c	Default	P2	CP	0.076	0.056			
13a	Default	Never	***CP***	***0.058***	***0.071***	0.063	+0.040	4926
13d	Off	Always	CP	0.098	0.075			
Figure	Surface LH flux parameter	LH scheme ''off''	Domain	Mean (cm)	σ (cm)	RMSD (cm)	Bias (cm)	N
13a	Default	Never	Entire	***0.150***	***0.195***	0.070	+0.044	13412
18a	50% enhancement	Never	Entire	0.195	0.224			
13a	Default	Never	Entire	***0.190***	***0.204***	0.149	−0.109	10415
18b	Default	P2	Entire	0.082	0.131			
13a	Default	Never	Entire	***0.190***	***0.204***	0.232	−0.163	10415
18c	Off	Always	Entire	0.028	0.060			
13a	Default	Never	CP	***0.067***	***0.072***	0.054	+0.042	4245
18a	50% enhancement	Never	CP	0.110	0.084			
13a	Default	Never	CP	***0.096***	***0.073***	0.102	−0.084	2817
18b	Default	P2	CP	0.013	0.024			
13a	Default	Never	CP	***0.096***	***0.073***	0.119	−0.095	2817
18c	Off	Always	CP	0.001	0.004			

collocation allows for the maximum projection of energy forced by underlying terrain features onto the realized convective cloud bands evident by the wide horizontal spacing and large cloud mixing ratios shown in Fig. 15b.

Vertical sections located downstream of the Cumberland Plateau in the 1.5-km domain normal to the banding (see Fig. 15b for reference) valid at 2100 UTC 6 December 2010 indicate differences in intensity of the bands generated by the two extreme surface SH flux experiments (Fig. 17). The enhanced surface SH flux experiment in Fig. 17a shows only a single band having a cloud mixing ratio exceeding 10×10^{-5} kg kg^{-1} and an associated cross-band low-level convergence and upper-level divergence exceeding -2×10^{-4} and $+4 \times 10^{-4}$ s^{-1}, respectively. All other bands in this simulation have lower cloud mixing ratios and weaker corresponding cross-band low-level convergence and upper-level divergence. In contrast, the zero-surface SH flux experiment section in Fig. 17b shows four bands having cloud mixing ratios exceeding 10×10^{-5} kg kg^{-1} and associated cross-band low-level convergence and upper-level divergence patterns exceeding -4×10^{-4} and $+4 \times 10^{-4}$ s^{-1}, respectively. The middle band is particularly strong, having a cloud mixing ratio exceeding 15×10^{-5} kg kg^{-1} and an associated low-level convergence zone exceeding -6×10^{-4} s^{-1}. The strength of this band is also evident by the wide horizontal spacing between it and the adjacent bands, indicative of strong compensating subsidence.

b. Surface latent heat flux experiments

The purpose of the surface latent heat flux experiments is to examine the source of the vapor that ultimately fell as snow accumulation in the SAMs region on 6/7 December 2010. Was this moisture carried from great distances already ''contained'' in the flow as parcels moved toward the SAMs, or did it originate from nearby soil having elevated moisture content that had been conditioned by a recent rainstorm? For each of the experiments applied to the December 2010 case study, the direction of the latent heat fluxes (not shown) is almost continually such that moisture is being lost by the ground to the drier atmosphere when the land surface

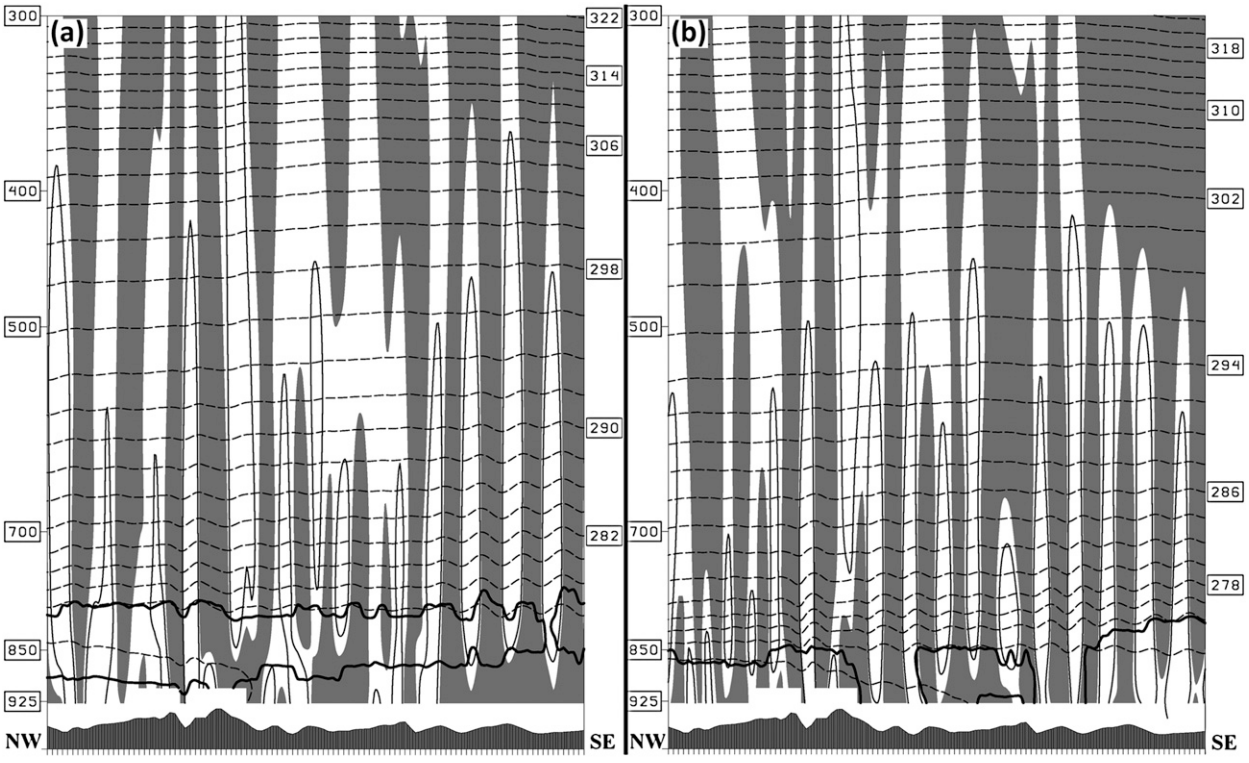

FIG. 14. As in Fig. 12, but for the (a) enhanced SH flux parameterization scheme turned on and (b) SH fluxes shut off during the entire model simulation in a vertical cross section oriented along the cloud band labeled NW–SE in Fig. 10b.

model is on. Therefore, the enhanced latent heat flux experiments generally increase the specific humidity of the PBL compared to the default simulations. The latent heating denial impacts are comparable to the effects of the enhanced sensible heating experiments described earlier. Each opposes the development of clouds and precipitation through either decreasing the available water vapor or through increasing the mean temperature (saturation vapor pressure) in the BL.

The model-simulated 24-h liquid equivalent accumulated precipitation in the 1.5-km domain during P34 is shown for three surface LH flux experiments in Fig. 18

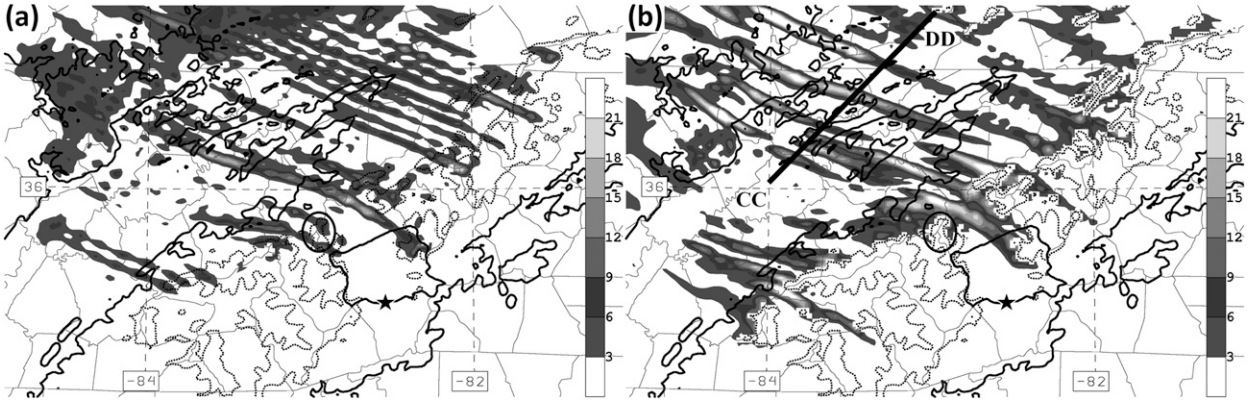

FIG. 15. Innermost (1.5 km) domain model simulated liquid and ice mixing ratio (shading, $\times 10^{-2}$ g kg^{-1}) and terrain elevation exceeding 0.4 (thick solid contours) and 1.0 km (dotted) valid at 2100 UTC 6 Dec (F21) at (a) the 825-hPa level for the enhanced and (b) the 900-hPa level for the zero-surface SH flux experiments. Line marked CC–DD in (b) is the orientation of the vertical cross section shown in Fig. 17. The borders of Buncombe County are thickened and the star symbol highlights the location of KAVL at the southern boundary of the county. The location of Max Patch is indicated by an oval to the northwest of Buncombe County.

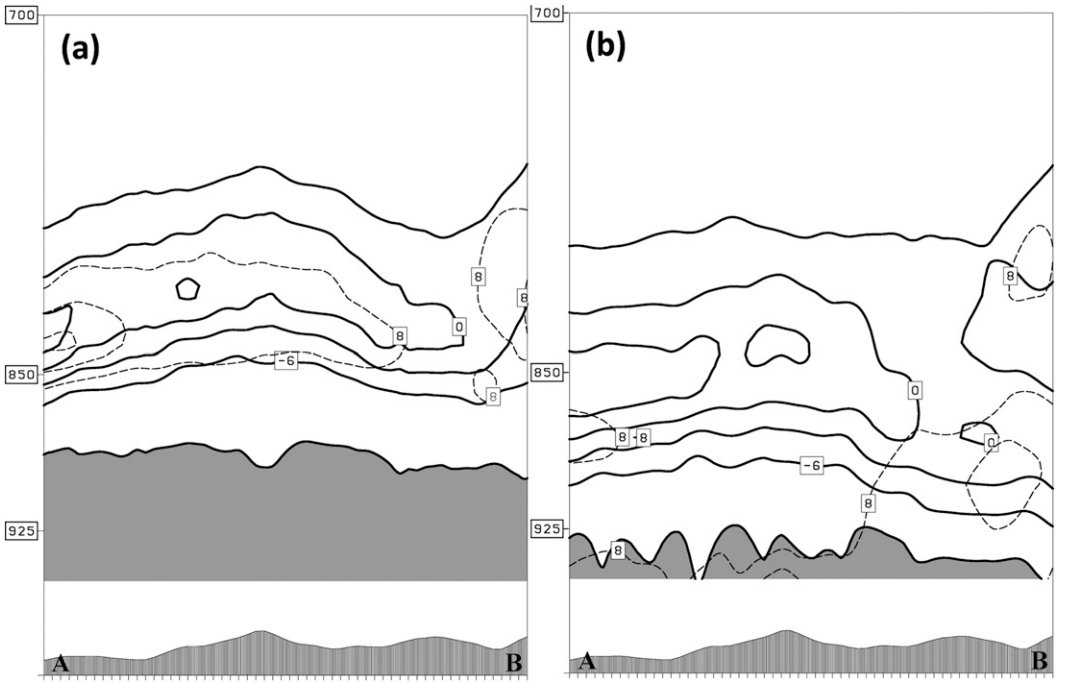

FIG. 16. Middle (4.5 km) domain model simulated environmental lapse rate (contoured in solid lines every 3°C km^{-1}) and wind shear (contoured in dashed lines; 8 and 12 × 10^{-3} s^{-1}) with steep lapse rates (magnitude >9°C km^{-1}) shaded valid at 1800 UTC 6 December [F18] for the (a) enhanced and (b) zero-surface SH flux experiments. Section A–B's location is highlighted in Fig. 2a.

and should be compared to the default simulation map plotted in Fig. 13a. Not surprisingly, enhanced surface LH fluxes bring air parcels to saturation sooner, resulting in accumulation increases in both the Cumberland Plateau and near the crest of the Great Smoky Mountains (Fig. 18a). Shutting surface LH fluxes off during daytime hours (P2, Fig. 18b) gives significantly reduced accumulation results across the entire domain. The experiment having surface LH fluxes shut off during the entire model simulation (Fig. 18c) shows the amount of snowfall that can be attributed to moisture packets carried great distances to the SAMs.

A statistical comparison between the no LH flux simulation of Fig. 18c and the default simulation (fifth and sixth rows in Table 1) leads to the conclusion that a substantial portion of the water mass that accumulates as snow over the mountains in the default simulation is evaporated or sublimated from the surface en route to the southern Appalachians. A comparison between the simulation in which surface LH fluxes are off during P2 and the default simulation (third and fourth rows, Table 1) shows a significant fraction of the water mass that fell during P34 in the default simulation was evaporated or sublimated from the surface during the daylight hours. It is possible that the importance of P2 surface LH fluxes is due to abundant surface moisture available over Kentucky and Tennessee, the P2 period corresponds to the time when mixing in the boundary layer is likely to be maximized, and/or because the migration of the vorticity maximum at the 500-hPa level leads to the greatest cyclonic vorticity advection during P2, generating ''deep'' synoptic-scale lift.

To address this ambiguity of interpretation, a trajectory analysis was completed for several sets of air parcels centered in time on the ''peaks'' of snowfall accumulation occurring during P34, as indicated in Fig. 7 (some trajectory paths not shown). The endpoints of the trajectories correspond to the 850-hPa level at the AA, BB, and ''Mid'' locations in Fig. 11 at F24 (0000 UTC 7 December 2010), F27, F30, F39, F42, and F45, for a total of 18 air parcel trajectory analyses. In all cases, air parcels arriving at the three locations at the six different times remained within the BL and increased their vapor mixing ratio as they traveled through the study domain. In 15 of 18 trajectories analyzed, the greatest increase in vapor mixing ratio occurred around 1900 UTC 6 December 2010 (F19). For the remaining three trajectories, the greatest increase occurred 24 h later, around 1900 UTC 7 December 2010 (F43). These times correspond to the second half of the daylight hours (see Fig. 7 for reference), the period when BL mixing would be maximized just before the sun begins to set.

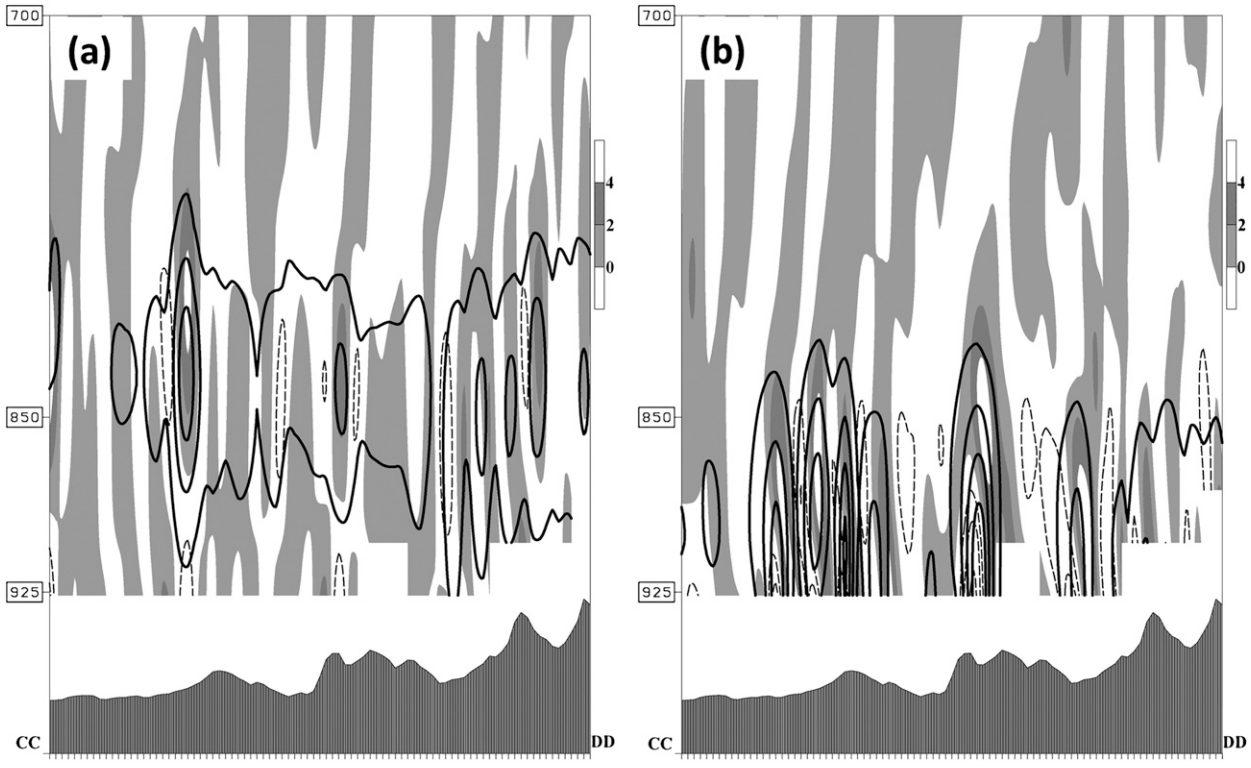

FIG. 17. Innermost (1.5 km) domain model simulated cloud mixing ratio (contoured in thick solid lines; 1, 5, 10, and 15×10^{-2} g kg^{-1}) and divergence of cross-band winds (divergence is shaded and convergence contoured in dashed lines; -2, -4, and -6×10^{-4} s^{-1}) valid at 2100 UTC 6 December [F21] for the (a) enhanced and (b) zero-surface SH flux experiments. Section CC–DD's location is highlighted in Fig. 15b.

Analysis of banding for the surface LH flux experiments (figures not shown) indicates that the simulations have band intensities no stronger than that in the enhanced surface SH flux experiment (Fig. 17a), in terms of cross-band divergence, differing only primarily in cloud mixing ratio. The layer of strongest unidirectional vertical wind shear in all of the surface LH flux experiments is well elevated above the orography (at about the 850-hPa level) and coincides with the inversion capping the PBL, similar to what is depicted in Fig. 16a, upstream of the Cumberland Plateau.

5. Summary

An early season northwest flow snowfall event impacting the southern Appalachian Mountains in western North Carolina has been examined to determine the near-term effects of the surface fluxes of moisture and heat on the 24-h accumulation of snowfall that occurred from 0000 UTC 7 December through 0000 UTC 8 December 2010 using atmospheric mesoscale model simulations of several experiments. This particular weather event was chosen for study because it occurred at a time when both types of surface fluxes might have played an important role in precipitation formation (the ground was not yet frozen). The purpose of this study was to investigate the potential impact of antecedent surface conditions directly upstream of the SAMs and the influence of diurnal effects in the PBL on the intensity of cloud and precipitation formation during NWFS events through experiments using the ARW-WRF mesoscale model.

WRF surface LH flux model experiments indicate that the origin of most of the moisture converted into snowfall accumulation in the southern Appalachians during this event came from the ground as air parcels traveled over the study domain toward the mountains. Trajectory analyses indicate that air parcels involved in the cloud and precipitation formation received the bulk of their water vapor in the PBL during daytime hours. WRF surface SH flux model experiments suggest that the *suppression* of surface sensible heat fluxes generally *increases* the simulated snowfall accumulation amounts. The daytime surface sensible heat fluxes partly oppose cloud development through the resultant heating and thickening of the PBL. However, the enhanced daytime mixing in the PBL also acts to efficiently transport moisture away from the ground, contributing to the

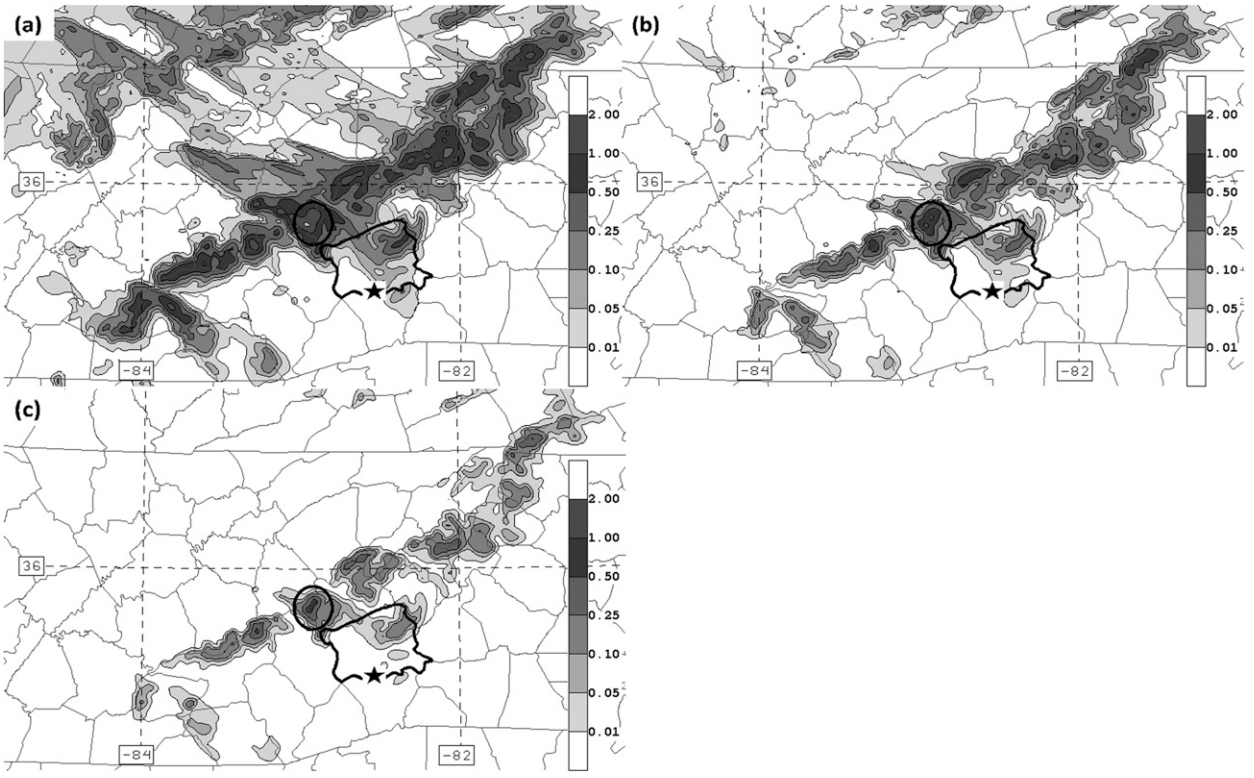

FIG. 18. Innermost (1.5 km) domain model simulated 24-h liquid equivalent accumulated precipitation (cm) for the period ending 0000 UTC 8 Dec 2010 (period designated P34) for the surface LH flux parameterization experiments having the (a) enhanced LH flux parameterization scheme on during the entire model simulation, (b) default LH flux parameterization scheme off during P2, and (c) LH fluxes shut off during the entire model simulation. The borders of Buncombe County are thickened and the star symbol highlights the location of KAVL at the southern boundary of the county. The location of Max Patch is indicated by an oval to the northwest of Buncombe County.

moistening of air parcels in the PBL and working in concert with cloud development at the top of the PBL.

The simulated banding for this particular case study is sensitive to the strength and vertical location of the layers of unidirectional vertical wind shear and dry-adiabatic lapse rates upstream of the mountains. The strongest banding, defined by both the maxima in cloud mixing ratio and magnitude of cross-band convergence, occurs under the conditions when the strongest unidirectional vertical wind shear is collocated within a layer having a nearly dry-adiabatic environmental lapse rate next to the ground. The collocation of these layers is only possible when the PBL depth is relatively shallow (simulated inversion base at ~875-hPa level). As the daytime buoyancy-driven PBL mixing increases in strength, the strong near-surface vertical wind shear layer is diminished and the layer of strongest unidirectional vertical wind shear ''lifts'' to, and is collocated with, the inversion layer capping the PBL. Since the inversion layer is located at a relatively high elevation above the ground, it ''feels'' the impact of the underlying mountains to a lesser degree than when the shear layer is next to the ground. As a result, the longitudinal banding becomes less sensitive to the underlying topography when the layer of strongest unidirectional vertical wind shear is found near the top of the PBL.

Operational near-term forecasting implications of this study related to the accurate prediction of northwest flow snowfall (NWFS) accumulations are to focus on several aspects of the PBL as the event unfolds. Based on the numerical experiments presented in this study, evolution of the PBL temperature, moisture, depth, wind profile, and stability are important factors in determining the production of clouds and precipitation at the top of the PBL during NWFS events. Specifically, cloud and snow production at the top of the PBL will be suppressed if the PBL is too warm, too dry, too thin, or too deep. The optimal condition for creating productive snow clouds in the upper PBL is to have cool PBL air (low-saturation vapor pressure) that quickly becomes saturated when water vapor is added to it via upward latent heat fluxes. The moistening of the PBL occurs

most efficiently when the PBL mixing, driven by shear- and/or buoyancy-produced turbulence, is of moderate strength. The PBL mixing cannot be too strong or the depth of the PBL will become too great and the low-level wind shear will be reduced so that the collocation of the most unstable air near the ground and layer of strongest vertical wind shear will be lost, diminishing the depth of the PBL longitudinal cloud bands and the corresponding snowfall production. If deep PBL longitudinal clouds can be maintained through optimal PBL conditions, the likelihood of significant snowfall accumulation occurring downstream of the crest of the mountains is increased. Optimal PBL conditions for producing intense longitudinal cloud bands are most likely to occur during nighttime hours.

Other operational near-term forecasting implications of this study related to the impact of errors in model estimates of surface moisture and heat fluxes upstream of the southern Appalachian Mountains on NWFS accumulation predictions are that LH underestimates and/or SH overestimates will contribute to suppressed cloud development and an underprediction of snowfall accumulation. In addition, these surface flux errors could result in erroneous predictions of high-impact warning areas being too narrowly confined to the primary southern Appalachian Mountains crest located along the eastern Tennessee and western North Carolina border. The implication is that a comparison of model-initialized fields of soil moisture and ground temperature to available observations upstream of the SAMs can provide a means for estimating the potential for these types of errors in model surface flux predictions and alert the forecaster to potentially misleading NWFS model simulations.

Of interest in future related studies will be to examine a prolonged NWFS case study in the absence of significant midtropospheric vorticity advection, allowing a study that better isolates the diurnal effects on the evolution of cloud and precipitation production. Analysis of additional NWFS case studies is needed to confirm what has been suggested in this study: that near-term moisture fluxes are significant contributors to the snowfall accumulations observed near the mountains of western North Carolina.

Acknowledgments. Funding for this project was provided in part by a UNC–GA research competitiveness grant, by a Renaissance Computing Institute grant, and by UNC Asheville undergraduate research grants. This research used the resources of the National Energy Research Scientific Computing Center, which is supported by the Office of Science of the U.S. Department of Energy under Contract DE-AC02-05CH11231. The author would like to thank the helpful contributions of Mr. Stephen Keighton, Dr. Gary Lackmann, Mr. Laurence Lee, and Dr. Baker Perry along with those of several anonymous reviewers whose comments greatly improved the quality of the manuscript. Finally, the author wishes to thank Dr. Phil Durkee and Mr. Richard Lind of the Naval Postgraduate School for loaning the sounding unit used during related wintertime field observation experiments over the past six cool seasons and for offering technical expertise in its operation.

REFERENCES

Brown, R. A., 1980: Longitudinal instabilities and secondary flows in the planetary boundary layer: A review. *Rev. Geophys. Space Phys.,* **18,** 683–697.

Draxler, R. R., and G. D. Hess, 1997: Description of the HYSPLIT_4 modeling system. NOAA Tech. Memo. ERL ARL-224, 24 pp.

——, and ——, 1998: An overview of the HYSPLIT_4 modeling system for trajectories, dispersion, and deposition. *Aust. Meteor. Mag.,* **47,** 295–308.

Durran, D. R., 1986: Mountain waves. *Mesoscale Meteorology and Forecasting,* P. S. Ray, Ed., Amer. Meteor. Soc., 472–492.

Fukuta, N., and T. Takahashi, 1999: The growth of atmospheric ice crystals: A summary of findings in vertical supercooled cloud tunnel studies. *J. Atmos. Sci.,* **56,** 1963–1979.

Holloway, B. S., 2007: The role of the Great Lakes in northwest flow snowfall events in the southern Appalachian Mountains. M.S. thesis, Dept. of Marine, Earth, and Atmospheric Sciences, North Carolina State University, 204 pp. [Available online at http://www.lib.ncsu.edu/theses/available/etd-11022007-181739/.]

Hong, S.-Y., and J.-O. J. Lim, 2006: The WRF single-moment 6-class microphysics scheme (WSM6). *J. Korean Meteor. Soc.,* **42,** 129–151.

——, J. Dudhia, and S.-H. Chen, 2004: A revised approach to ice microphysical processes for the bulk parameterization of clouds and precipitation. *Mon. Wea. Rev.,* **132,** 103–120.

——, Y. Noh, and J. Dudhia, 2006: A new vertical diffusion package with an explicit treatment of entrainment processes. *Mon. Wea. Rev.,* **134,** 2318–2341.

Hudgins, J., 2008: Mesoscale snowbands persisting downstream of the southern Appalachians during northwest flow upslope events. *33rd National Weather Association Annual Meeting,* Louisville, KY, NWA, P3.4. [Available online at http://www.nwas.org/meetings/abstracts/display.php?id=306.]

Janjić, Z. I., 1994: The step-mountain eta coordinate model: Further developments of the convection, viscous sublayer and turbulence closure schemes. *Mon. Wea. Rev.,* **122,** 927–945.

——, 2000: Comments on ''Development and evaluation of a convection scheme for use in climate models.'' *J. Atmos. Sci.,* **57,** 3686.

Keighton, S., and Coauthors, 2009: A collaborative approach to study northwest flow snow in the southern Appalachians. *Bull. Amer. Meteor. Soc.,* **90,** 979–991.

Kirshbaum, D. J., and D. R. Durran, 2005: Atmospheric factors governing banded orographic convection. *J. Atmos. Sci.,* **62,** 3758–3774.

——, G. H. Bryan, R. Rotunno, and D. R. Durran, 2007a: The triggering of orographic rainbands by small-scale topography. *J. Atmos. Sci.,* **64,** 1530–1549.

——, R. Rotunno, and G. H. Bryan, 2007b: The spacing of orographic rainbands triggered by small-scale topography. *J. Atmos. Sci.,* **64,** 4222–4245.

Lackmann, G. M., 2001: Analysis of a surprise western New York snowstorm. *Wea. Forecasting,* **16,** 99–116.

Mesinger, F., and Coauthors, 2006: North American Regional Reanalysis. *Bull. Amer. Meteor. Soc.,* **87,** 343–360.

Mlawer, E. J., S. J. Taubman, P. D. Brown, M. J. Iacono, and S. A. Clough, 1997: Radiative transfer for inhomogeneous atmosphere: RRTM, a validated correlated-k model for the longwave. *J. Geophys. Res.,* **102** (D14), 16 663–16 682.

NCDC, 2010a: *Storm Data.* Vol. 52, No. 11, 166 pp.

——, 2010b: *Storm Data.* Vol. 52, No. 12, 242 pp.

Perry, L. B., 2006: Synoptic climatology of northwest flow snowfall in the southern Appalachians. Ph.D. dissertation, University of North Carolina at Chapel Hill, 176 pp. [Available online at http://dc.lib.unc.edu/u?/etd,165.]

——, and C. E. Konrad, 2006: Relationships between NW flow snowfall and topography in the southern Appalachians, USA. *Climate Res.,* **32,** 35–47.

——, ——, and T. W. Schmidlin, 2007: Antecedent upstream air trajectories associated with northwest flow snowfall in the southern Appalachians. *Wea. Forecasting,* **22,** 334–352.

——, D. K. Miller, S. E. Yuter, L. G. Lee, and S. J. Keighton, 2008: Atmospheric influences on new snowfall density in the southern Appalachian Mountains, USA. *Proc. 65th Eastern Snow Conf.,* Fairlee, VT, Eastern Snow Conference, 123–133. [Available online at http://www.easternsnow.org/proceedings/2008/perry_et_al.pdf.]

——, C. E. Konrad, D. Hotz, and L. G. Lee, 2010: Synoptic classification of snowfall events in the Great Smoky Mountains, USA. *Phys. Geogr.,* **31,** 156–171.

Pruppacher, H. R., and J. D. Klett, 1997: *Microphysics of Clouds and Precipitation.* 2nd ed. D. Reidel, 714 pp.

Rozumalski, R. A., 2007: WRF Environmental Modeling System user's guide: Demystifying the process of installing, configuring, and running the Weather Research and Forecasting model. NOAA/NWS Forecast Decision Training Branch, COMET/UCAR, 95 pp. [Available online at http://strc.comet.ucar.edu/wrf/wrfems_userguide.htm.]

Ryan, B. F., E. R. Wishart, and D. E. Shaw, 1976: The growth rates and densities of ice crystals between −3°C and −21°C. *J. Atmos. Sci.,* **33,** 842–850.

Schmidlin, T. W., 1992: Does lake-effect snow extend to the mountains of West Virginia? *Proc. 49th Eastern Snow Conf.,* Oswego, NY, Eastern Snow Conference, 145–148.

Scorer, R., 1949: Theory of waves in the lee of mountains. *Quart. J. Roy. Meteor. Soc.,* **75,** 41–56.

Skamarock, W. C., and Coauthors, 2008: A description of the Advanced Research WRF version 3. NCAR Tech. Note NCAR/TN-475+STR, 88 pp. [Available online at http://www.mmm.ucar.edu/wrf/users/docs/arw_v3.pdf.]

Sousounis, P. J., 2001: Lake effect storms. *Encyclopedia of Atmospheric Sciences,* J. Holton, J. Pyle, and J. Curry, Eds., Academic Press, 1104–1115.

——, and M. J. Fritsch, 1994: Lake-aggregate mesoscale disturbances. Part II: A case study of the effects on regional and synoptic-scale weather systems. *Bull. Amer. Meteor. Soc.,* **75,** 1793–1811.

Stearns, C. R., and G. A. Weidner, 1993: Sensible and latent heat flux estimates in Antarctica. *Antarctic Meteorology and Climatology: Studies Based on Automatic Weather Stations,* D. H. Bromwich and C. R. Stearns, Eds., Antarctic Research Series, Vol. 61, Amer. Geophys. Union, 109–138.

Stull, R. B., 1988: *An Introduction to Boundary Layer Meteorology.* Kluwer Academic, 666 pp.

Weckwerth, T. M., T. W. Horst, and J. W. Wilson, 1999: An observational study of the evolution of horizontal convective rolls. *Mon. Wea. Rev.,* **127,** 2160–2179.

Yoshizaki, M., T. Kato, Y. Tanaka, H. Takayama, Y. Shoji, and H. Seko, 2000: Analytical and numerical study of the 26 June 1998 orographic rainband observed in western Kyushu, Japan. *J. Meteor. Soc. Japan,* **78,** 835–856.

Young, G. S., D. A. R. Kristovich, M. R. Hjelmfelt, and R. C. Foster, 2002: Rolls, streets, waves, and more: A review of quasi-two-dimensional structures in the atmospheric boundary layer. *Bull. Amer. Meteor. Soc.,* **83,** 997–1001.

Yuter, S. E., and L. B. Perry, 2007: Storm structures and precipitation characteristics of snow events in the southern Appalachian Mountains. Preprints, *12th Conf. on Mesoscale Processes,* Waterville Valley, NH, Amer. Meteor. Soc., P2.14. [Available online at https://ams.confex.com/ams/12meso/techprogram/paper_126103.htm.]